引用格式：YANG Ruimu, DONG Xiaopeng. A Modified Three-wavelength Demodulation Method for Small Signals of EFPI [J]. Acta Photonica Sinica, 2023, 52(8):0806002
杨芮牧,董小鹏.一种改进的三波长EFPI小信号解调方法[J].光子学报,2023,52(8):0806002

一种改进的三波长EFPI小信号解调方法

杨芮牧,董小鹏
(厦门大学 电子科学与技术学院 光波技术研究所,厦门 361000)

摘　要:针对非本征法布里-珀罗干涉型(EFPI)传感器采用对称三波长解调法检测小信号时可能存在的波形变差问题,提出一种针对小信号的改进的对称三波长解调方法。利用三角函数的小信号近似,得到简化的公式计算求出三路信号的相位差,解决EFPI干涉信号的衰落问题。仿真与实验结果表明,该方法在针对小信号解调方面比现有三波长法具有更高的算法稳定性与更小的误差,同时在低信噪比的场景下对波形具有更好的恢复效果。实验上分别用本文方法和现有方法对相同声波信号进行解调,本文方法解调的信噪比较现有方法高12 dB以上。

关键词:非本征法布里-珀罗干涉仪;三波长解调;信号衰落;声波检测;小信号
中图分类号:TN29　　**文献标识码**:A　　**doi**:10.3788/gzxb20235208.0806002

0　引言

光纤非本征法布里-珀罗干涉仪(Extrinsic Fabry-Perot interferometers, EFPI)作为光纤干涉仪的一种,具有抗电磁干扰、体积小、成本低、灵敏度高、相位一致性高[1]等特点,在声波检测场景中,如光纤水听器、无源测向、基于光声效应的气体检测、表面声波应变传感等方面有许多应用[2-6]。EFPI可以看作是一个信号调制器件,将外界振动信号调制在EFPI的干涉光上,EFPI腔长的变化导致干涉光强的变化,完成信号的调制之后输出。然而,EFPI传感器的腔长对环境变量,如温度、气压等参量极为敏感,腔长变化引起的正交工作点漂移会导致信号的衰落与畸变。针对干涉仪输出信号的衰落问题,2005年,王民裕等[7]提出采用特定波长间隔的双波长光源,克服光纤Mach-Zehnder干涉仪偏置漂移引起的信号衰落问题,但这种双波长法在EFPI腔长变化较大时不适用。其它解调方法在小信号的情况下实用性较差甚至失效,例如:椭圆拟合法在小信号情况下,绘制出的李萨如椭圆会退化为一条直线,并且还有实时性差、解调速度慢的缺点[8-9];二阶微分交叉相乘算法(Differentiate-and-Cross-Multiply, DCM)具有广泛的适用性,但必须准确去除直流项[10],而对于小信号来说,直流的去除难以实现[11];贝塞尔比值法存在同样的困难且只能解调单频信号[12-13];采用可调谐激光器反馈控制正交偏置点的方法存在成本高的问题[14],具有波长扫描功能的激光器对硬件可靠性有较高要求[10];相位生成载波(Phase Generated Carrier, PGC)技术需要复杂的载波调制系统,频率响应范围有限[15],且PGC采用压电换能生成相位载波时系统复杂、体积较大[16]。相比之下,强度解调方法具有信号处理较为简单、灵敏度高等优点,适合高速和小信号声波的检测[12]。

2020年江毅等[17]提出了一种适用于不稳定腔长和未知腔长的对称三波长解调方法(Symmetrical demodulation method, SDM),通过选择特定的三个波长来构建三路输出信号之间两个相等的干涉相位差,之后再通过数学运算恢复信号的相位,其拥有动态范围大、运算简单等优点,较适合大信号的检测。但在小信号情况下,尤其在系统或环境噪声较大时,SDM算法有可能导致解调结果噪声和误差增加。为此,本文针对小信号检测情况提出一种改进的三波长解调方法(Modified Symmetrical Demodulation method, MSDM),

基金项目:国家自然科学基金(No. 61775186),厦门市海洋发展局(No. 16CZB025SF03),厦门市光通讯器件测试重点实验室项目
第一作者:杨芮牧,1826210704@qq.com
通讯作者:董小鹏,xpd@xmu.edu.cn
收稿日期:2023-02-28;**录用日期**:2023-04-04

在现有SDM构建的三路输出信号基础上，重新构建两路强度可以互相补偿的中间量，从而得到一个波形更好的强度解调结果。本文通过仿真与实验，对SDM与MSDM解调的结果进行对比，验证了新方法在小信号解调方面的优越性。在信噪比较差的小信号情况下，该方法具有更好的算法稳定性与输出结果。

1 基本原理

本文实验系统结构如图1所示。与文献[17]采用激光器的方案不同，我们采用宽带光源加三个特定波长的滤波器实现三波长解调。宽带光源发出的光经过环形器之后到达EFPI传感器，扬声器产生的声波信号会调制到EFPI返回的干涉信号上，干涉信号通过环形器后进入1×3耦合器分为三束光，经过工作波长分别为λ_1、λ_2、λ_3的三个窄带滤波器，再进入光电探测器(Photoelectric detector, PD)及信号放大电路、采集卡与计算机(Personal computer, PC)。PD单元将光信号转换为电信号，PC上的软件对采集卡采集到的信号进行解调，并最终还原出声波振动信号。

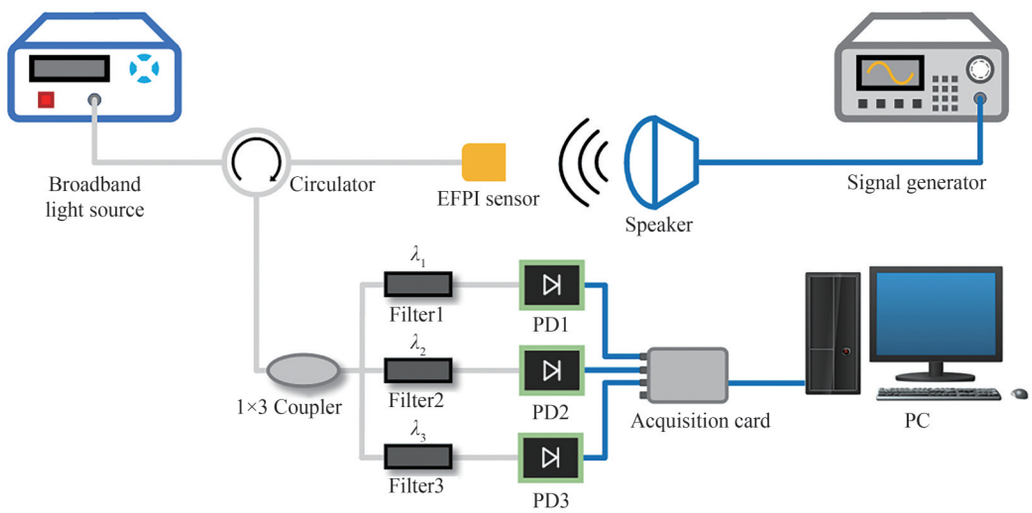

图1 改进的三波长解调方法系统原理图

Fig. 1 Schematic diagram of MSDM demodulation system

本实验制作的EFPI传感器的结构见图2(a)。构成EFPI的两个反射面一个为光纤平端面，另一个为弹性膜片，光射入EFPI后，两端面的反射光叠加后将会产生干涉。当声波作用于膜片时，声压会导致膜片变形并改变EFPI传感器的腔体长度，腔体长度的变化导致干涉光强度变化，实现声波对振动信号的调制，之后通过EFPI反射的干涉光强度变化实现对声音的传感。

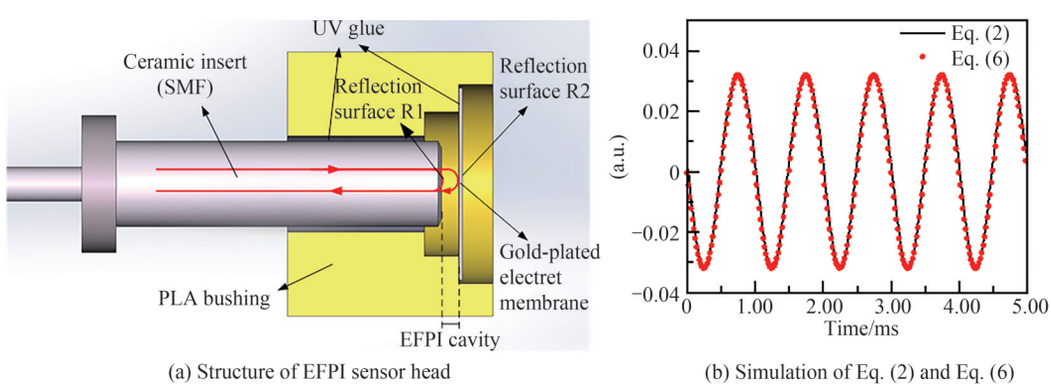

(a) Structure of EFPI sensor head (b) Simulation of Eq. (2) and Eq. (6)

图2 EFPI传感器结构与式(2)式(6)仿真

Fig. 2 Structure of EFPI sensor head and simulation of Eq. (2) and Eq. (6)

EFPI的双光束干涉信号为

$$r = r_{\text{front}} + r_{\text{back}} + 2\sqrt{r_{\text{front}} r_{\text{back}}}\cos\left(\frac{4\pi nL}{\lambda}\right) \tag{1}$$

式中，r_{front}、r_{back}分别是EFPI前后反射面的反射光强，分别由光纤端面与膜片反射，n是腔内介质的折射率（空气情况下为1），L是EFPI的腔长，L会随着环境（如温度、气压）等随机变化，造成信号的衰落。令$D = r_{\text{front}} + r_{\text{back}}$，$B = 2\sqrt{r_{\text{front}} r_{\text{back}}}$，选择特定的波长$\lambda_1$、$\lambda_2$、$\lambda_3$并在三路信号之间构建两两相等的相位差[17]，即$\delta = 4\pi n\big(L + s(t)\big)\dfrac{\lambda_1 - \lambda_2}{\lambda_1\lambda_2} = 4\pi n\big(L + s(t)\big)\dfrac{\lambda_2 - \lambda_3}{\lambda_2\lambda_3}$，$s(t)$为EFPI接收到的外界振动信号，通常情况下该信号为正弦信号，$s(t)$调制后的干涉光可以表示为

$$r_k = D + B\cos\left(\frac{4\pi nL}{\lambda_k} + \frac{4\pi ns(t)}{\lambda_k}\right) = D + B\cos\left(\frac{4\pi nL}{\lambda_k}\right)\cos\left(\frac{4\pi ns(t)}{\lambda_k}\right) - B\sin\left(\frac{4\pi nL}{\lambda_k}\right)\sin\left(\frac{4\pi ns(t)}{\lambda_k}\right), k = 1, 2, 3 \tag{2}$$

在已有的SDM中，信号的解调需要计算以下中间量[17]

$$\begin{cases} R_1 = r_2 - \dfrac{r_1 + r_3}{2} \\ R_2 = \dfrac{r_1 - r_3}{2} \end{cases} \tag{3}$$

$$C = \frac{A_R}{A_r} = 1 - \cos\delta \tag{4}$$

$$\begin{cases} \varphi_t = \pm\arctan\dfrac{CR_2}{\sqrt{2C - C^2}\cdot R_1} \\ d_t = \dfrac{\lambda_2}{4n\pi}\varphi_t \end{cases} \tag{5}$$

式中，A_R、A_r分别为R_1与r_2交流部分的幅值，$\varphi_t = \dfrac{4\pi nL}{\lambda_2} + \dfrac{4\pi ns(t)}{\lambda_2}$，$d_t = L + s(t)$为解调后的腔长。当信号$s(t)$为小信号时，受限于采集卡的位数等硬件限制，中间量在计算过程中容易出现误差传递放大的情况：1）$s(t)$的幅值远小于1，$\cos\left(\dfrac{4\pi ns(t)}{\lambda_k}\right) \approx 1$[7]，此时$r_k$的直流项就变为$D + B\cos\left(\dfrac{4\pi nL}{\lambda_k}\right)$，这会导致小信号时式（2）直流的去除难以准确。理想情况下，即工作点$\dfrac{4\pi nL}{\lambda_k} = \dfrac{\pi}{2}$时，$r_k$的交流部分幅度占整个信号幅度的比值最大为24.26%，即$\dfrac{A_r}{D + B\cos\left(\dfrac{4\pi nL}{\lambda_k}\right)} \leqslant 24.26\%$，实际应用中$r_{\text{front}}$与$r_{\text{back}}$的不平衡、正交工作点漂移、噪声等因素都会导致该比值远不足24.26%，此时A_R与A_r的取值容易受到大数吃小数的影响而产生较大的误差，影响C值的获取；2）$r_2 \approx (r_1 + r_3)/2$，$R_1$的计算会出现相近数相减的情况，发生抵消现象，$R_1$的值很容易受到噪声的影响而变差，在式（5）的运算中，R_1做分母会导致φ_t的计算误差增大。

为了提高使用场景为小信号时解调算法的准确性与实用性，本文提出一种改进的解调方法：光源波长为1 550 nm时，EFPI反射的干涉光相位遍历0～2π，对应的腔长变化范围为775 nm，当信号振动幅度反映在干涉信号相位上的弧度值小于0.22 rad时，即振动引起的腔长变化小于30.11 nm时，$\sin x$与x的近似误差小于1%。此时对于式（2），去除直流部分$D + B\cos\left(\dfrac{4\pi nL}{\lambda_k}\right)$，同时做近似$\sin\left(\dfrac{4\pi ns(t)}{\lambda_k}\right) \approx \dfrac{4\pi ns(t)}{\lambda_k}$，得到三路信号的通式

$$I_k = B\sin\left(\frac{4\pi nL}{\lambda_k}\right)\frac{4\pi ns(t)}{\lambda_k}, k = 1, 2, 3 \tag{6}$$

图 2(b)为 $\frac{4\pi n\cdot\max\left(s(t)\right)}{\lambda_k}=x=0.2$ rad 的条件下式(2)与式(6)的仿真结果,图中式(2)已去除直流部分,从图中可以看出两式的交流部分具有良好的一致性,证明在接收信号为小信号情况下,式(6)可以作为式(2)的近似。记 $\frac{4\pi nL}{\lambda_2}=\varphi$,同样选择特定的波长 λ_1、λ_2、λ_3 在三路信号之间构建两两相等的相位差,则式(6)可以表示为

$$\begin{cases} I_1=B\sin(\varphi-\delta)\dfrac{4\pi ns(t)}{\lambda_1} \\ I_2=B\sin(\varphi)\dfrac{4\pi ns(t)}{\lambda_2} \\ I_3=B\sin(\varphi+\delta)\dfrac{4\pi ns(t)}{\lambda_3} \end{cases} \tag{7}$$

令

$$\alpha=\lambda_1 I_1+\lambda_3 I_3=2B\sin\varphi\cos\delta\cdot 4\pi ns(t) \tag{8}$$

则

$$\cos\delta=\frac{\alpha}{2\lambda_2 I_2}=\frac{2B\sin\varphi\cos\delta\cdot 4\pi ns(t)}{2B\sin\varphi\cdot 4\pi ns(t)} \tag{9}$$

$$\sin\delta=\sqrt{1-\cos^2\delta} \tag{10}$$

$$\beta=\lambda_1 I_1-\lambda_3 I_3=2B\cos\varphi\sin\delta\cdot 4\pi ns(t) \tag{11}$$

$$\sqrt{\left(\frac{\alpha}{\cos\delta}\right)^2+\left(\frac{\beta}{\sin\delta}\right)^2}=\sqrt{(2B\sin\varphi\cdot 4\pi ns(t))^2+(2B\cos\varphi\cdot 4\pi ns(t))^2}=2B\cdot 4\pi n|s(t)| \tag{12}$$

式(12)的结果需要做去绝对值处理:选取 α 与 β 中幅度较大的信号,做取符号运算即可得到

$$s(t)=\frac{\mathrm{sign}}{8B\pi n}\sqrt{\left(\frac{\alpha}{\cos\delta}\right)^2+\left(\frac{\beta}{\sin\delta}\right)^2}\quad \mathrm{sign}=\begin{cases}\mathrm{sgn}(\alpha),\max(\alpha)\geqslant\max(\beta)\\ \mathrm{sgn}(\beta),\max(\alpha)<\max(\beta)\end{cases} \tag{13}$$

2 算法稳定性分析

数值计算中,常用误差限和相对条件数来估计算法对误差的敏感性,高敏感性的算法被认为是不稳定的[18]。设式(2)中 r_k 的初始误差限为 $\varepsilon(r)$,即 $\varepsilon(r_k)=\varepsilon(r)$,同时记式(5)中 d_t 对 φ_t 的条件数为 $\mathrm{cond}(d_t)$,则 SDM 算法的误差限与条件数可由式(14)~(18)计算

$$\begin{cases}\varepsilon(R_1)=\varepsilon(r_2)+\dfrac{\varepsilon(r_1)+\varepsilon(r_3)}{2}=2\varepsilon(r)\\ \varepsilon(R_2)=\dfrac{\varepsilon(r_1)-\varepsilon(r_3)}{2}=\varepsilon(r)\end{cases} \tag{14}$$

$$\varepsilon(C)\approx\varepsilon\left(\frac{A_R}{A_r}\right)=\frac{|A_R|\varepsilon(A_r)+|A_r|\varepsilon(A_R)}{{A_r}^2}=\frac{|A_R|+2|A_r|}{{A_r}^2}\varepsilon(r) \tag{15}$$

$$\varepsilon\left(\frac{CR_2}{ER_1}\right)\approx\frac{|CR_2|\varepsilon(ER_1)+|ER_1|\varepsilon(CR_2)}{(ER_1)^2}=$$

$$\frac{|CR_2|\left(\sqrt{2C-C^2}\cdot 2\varepsilon(r)+|R_1|\cdot\dfrac{1-C}{\sqrt{2C-C^2}}|\cdot\varepsilon(C)\right)+|ER_1|(|C|\cdot\varepsilon(R_2)+|R_2|\cdot\varepsilon(C))}{(ER_1)^2} \tag{16}$$

$$\varepsilon(d_t)\approx\frac{\lambda_2}{4\pi}\cdot\frac{1}{1-\left(\dfrac{CR_2}{\sqrt{2C-C^2}\cdot R_1}\right)^2}\cdot\varepsilon\left(\frac{CR_2}{ER_1}\right) \tag{17}$$

$$\mathrm{cond}(d_t)\approx\left|\frac{\varphi_t}{d_t}\cdot\frac{\frac{\lambda_2}{4\pi}}{1+\left(\frac{CR_2}{ER_1}\right)^2}\cdot\left[\frac{d\left(\frac{CR_2}{ER_1}\right)}{dR_2}\cdot\frac{dR_2}{d\varphi_t}+\frac{d\left(\frac{CR_2}{ER_1}\right)}{dR_1}\cdot\frac{dR_1}{d\varphi_t}\right]\right|=$$
$$\left|\frac{\varphi_t}{d_t}\cdot\frac{1}{1+\left(\frac{CR_2}{ER_1}\right)^2}\cdot\left(\frac{C\cos(\varphi_t)}{R_1}+\frac{C^2R_2\sin(\varphi_t)}{ER_1{}^2}\right)\right| \tag{18}$$

图3(a)为SDM误差限$\varepsilon(d_t)$关于C的函数曲线，C的变化反映着腔长的变化，C是一个随着腔长L周期变化的值，取值范围为0～2。假设输入信号r_k的误差限$\varepsilon(r)$量级为10^{-1}，SDM运算的误差限$\varepsilon(d_t)$的数量级为10^{-5}。图3(b)为SDM的相对条件数$\mathrm{cond}(d_t)$在两个周期内的曲线，一个算法的相对条件数越接近1，其算法的稳定性越好，图3(b)中可以看出，随着φ_t变化，SDM的相对条件数同样不平稳，在最低处仍高达10^3数量级，这表示当SDM解调周期信号时，不同时刻的稳定性同样不同，会导致SDM解调波形变差。误差限与相对条件数分别从腔长(空域)与周期(时域)上反映了算法的敏感性。

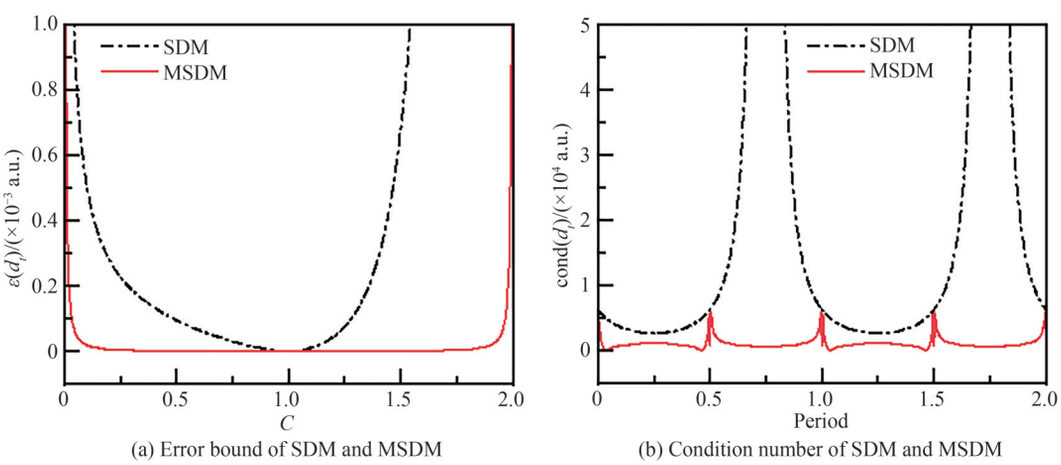

(a) Error bound of SDM and MSDM　(b) Condition number of SDM and MSDM

图3　SDM与MSDM的误差限与条件数

Fig. 3　Error bound and condition number of SDM and MSDM

MSDM由于舍弃了采集信号的直流部分，在采集卡等硬件设备垂直分辨率有限的情况下，可以达到对信号交流部分精度更高的采集，削弱大数吃小数现象；MSDM的α与β通过对I_1、I_3分别进行和与差的运算，保证中间量α与β的大小关系始终相反，使α与β中的至少一个拥有较大的幅值，不会在计算时同时发生抵消现象。同时，MSDM并未对α与β进行反三角函数等恢复相位的运算，由此将SDM的相位解调转换为强度解调，最终的平方和运算可以加大质量好的中间量的权重。同样地，对于MSDM设置I_k的初始误差限为$\varepsilon(r)$，$\varepsilon(I_k)=\varepsilon(r)$，$\mathrm{cond}\big(s(t)\big)$为式(13)中$s(t)$对$\varphi_t$的条件数，为了简化计算，做近似$\lambda_1\approx\lambda_3\approx\lambda_2$，MSDM算法的误差限与条件数可由式(19)～(25)计算。

$$\varepsilon(\cos\delta)\approx\varepsilon\left(\frac{\alpha}{2\lambda_2 I_2}\right)=\frac{|\alpha|\cdot2\lambda_2\varepsilon(\beta)+|2\lambda_2 I_2|\varepsilon(\alpha)}{|2\lambda_2 I_2|^2}=\frac{2}{|I_2|}\varepsilon(r) \tag{19}$$

$$\varepsilon(\sin\delta)=\varepsilon\left(\sqrt{1-\cos^2\delta}\right)\approx\left|\frac{\cos\delta}{\sqrt{1-\cos^2\delta}}\right|\varepsilon(\cos\delta) \tag{20}$$

$$\varepsilon\left(\frac{\alpha}{\cos\delta}\right)\approx\frac{\left|\lambda_2(I_1+I_3)\right|\cdot\frac{2}{|I_2|}\varepsilon(r)+\left|\frac{\lambda_2(I_1+I_3)}{2\lambda_2 I_2}\right|\cdot 2\lambda_2\varepsilon(r)}{\left|\frac{\lambda_2(I_1+I_3)}{2\lambda_2 I_2}\right|^2}\approx 6\lambda_2\varepsilon(r) \tag{21}$$

$$\varepsilon\left(\frac{\beta}{\sin\delta}\right)\approx\frac{|\lambda_2(I_1-I_3)|\varepsilon(\sin\delta)+\sqrt{1-\cos^2\delta}\cdot 2\lambda_2\varepsilon(r)}{1-\cos^2\delta} \tag{22}$$

$$\varepsilon\left(\left(\frac{\alpha}{\cos\delta}\right)^2+\left(\frac{\beta}{\sin\delta}\right)^2\right)\approx 2\left|\frac{\alpha}{\cos\delta}\right|\varepsilon\left(\frac{\beta}{\sin\delta}\right)+2\left|\frac{\beta}{\sin\delta}\right|\varepsilon\left(\frac{\alpha}{\cos\delta}\right) \tag{23}$$

$$\varepsilon(s(t))\approx\frac{1}{8\pi}\cdot\frac{1}{2\sqrt{\left(\frac{\alpha}{\cos\delta}\right)^2+\left(\frac{\beta}{\sin\delta}\right)^2}}\cdot\varepsilon\left(\left(\frac{\alpha}{\cos\delta}\right)^2+\left(\frac{\beta}{\sin\delta}\right)^2\right) \tag{24}$$

$$\begin{aligned}\mathrm{cond}(s(t))\approx\Bigg|&\frac{\varphi_t}{s(t)}\cdot\frac{\frac{1}{8\pi}}{2\sqrt{\left(\frac{\alpha}{\cos\delta}\right)^2+\left(\frac{\beta}{\sin\delta}\right)^2}}\cdot\\&\left(\frac{2\lambda_2\alpha}{\cos\delta}(-\sin(\varphi-\delta)-\sin(\varphi+\delta)+\frac{2\lambda_2\beta}{\sin\delta}\left(-\sin(\varphi-\delta)+\sin(\varphi+\delta)\right)\right)\Bigg|\end{aligned} \tag{25}$$

MSDM的误差限$\varepsilon\left(s(t)\right)$关于$C$的曲线和相对条件数$\mathrm{cond}\left(s(t)\right)$曲线分别见图3(a)(b)。$\varepsilon(r)$量级为$10^{-1}$时，MSDM的误差限$\varepsilon(s(t))$数量级为$10^{-7}$，对于SDM来说，微小误差对结果造成的扰动是MSDM的$10^{-5}/10^{-7}=100$倍。为了便于观察，图3(b)中MSDM的条件数曲线进行了100倍的放大，MSDM的相对条件数数量级$\mathrm{cond}\left(s(t)\right)$处于10左右且在信号周期内分布更加平坦，这表示MSDM相对于SDM具有更好的稳定性。

3 数值仿真

对两种方法分别进行数值仿真，三路信号的工作波长分别选取$\lambda_1=1\,540.56$ nm、$\lambda_2=1\,541.35$ nm、$\lambda_3=1\,542.14$ nm，仿真的虚拟声信号为1 kHz的正弦波，虚拟EFPI的腔长按5 μm的步长从50 μm变化至500 μm，输入EFPI的振动信号的空间幅度为10 nm，解调算法的解调误差随腔长变化见图4(a)，误差通过$(A_o-A_i)/A_i$计算，其中A_o是算法解调结果的幅值，A_i是输入信号的幅值。对于50～500 μm范围的腔长，MSDM解调误差在绝大多数情况下控制在0.2%以内，相比SDM误差更小且更加平稳。图4(a)中，SDM与MSDM在50 μm、200 μm、400 μm处出现了较大的误差波动，这是由于cosδ计算出现误差导致的，图4(b)可以看出，实际运算值$1-C$与其理论值cosδ之间的误差与腔长存在关系。在50 μm、200 μm、400 μm附近，MSDM的cosδ值计算相对更加准确，同时误差也更小。

图4(c)是对不同频率信号的解调误差，信号幅度为10 nm，腔长为200 μm，信号从10 Hz不均匀变化至100 kHz，此时MSDM解调误差绝大多数情况下保持在0.5%以下，且始终比SDM的误差小。当腔长固定为200 μm时，误差随振动信号的幅度变化见图4(d)，可见MSDM解调方法对于在振动幅度小于25 nm的小信号具有较小的误差且小于SDM误差；当振动幅度超过25 nm时，由于式(6)到式(2)近似关系的失效，MSDM的解调误差将会变得复杂，本方法失效。

进一步仿真两种方法对噪声的敏感性。分别对仿真的信号加入均值为0、方差为$0.02B$的高斯白噪声[19-20]，如图5(a)所示，黑色为将输入信号经过高斯平滑之后的波形。从图5(b)(c)可以看出，由于SDM的敏感性较高，SDM的解调结果在波峰波谷位置出现了较多的噪声信息。在同样的数据与预处理条件下，MSDM实现了对信号波形更优秀的还原。

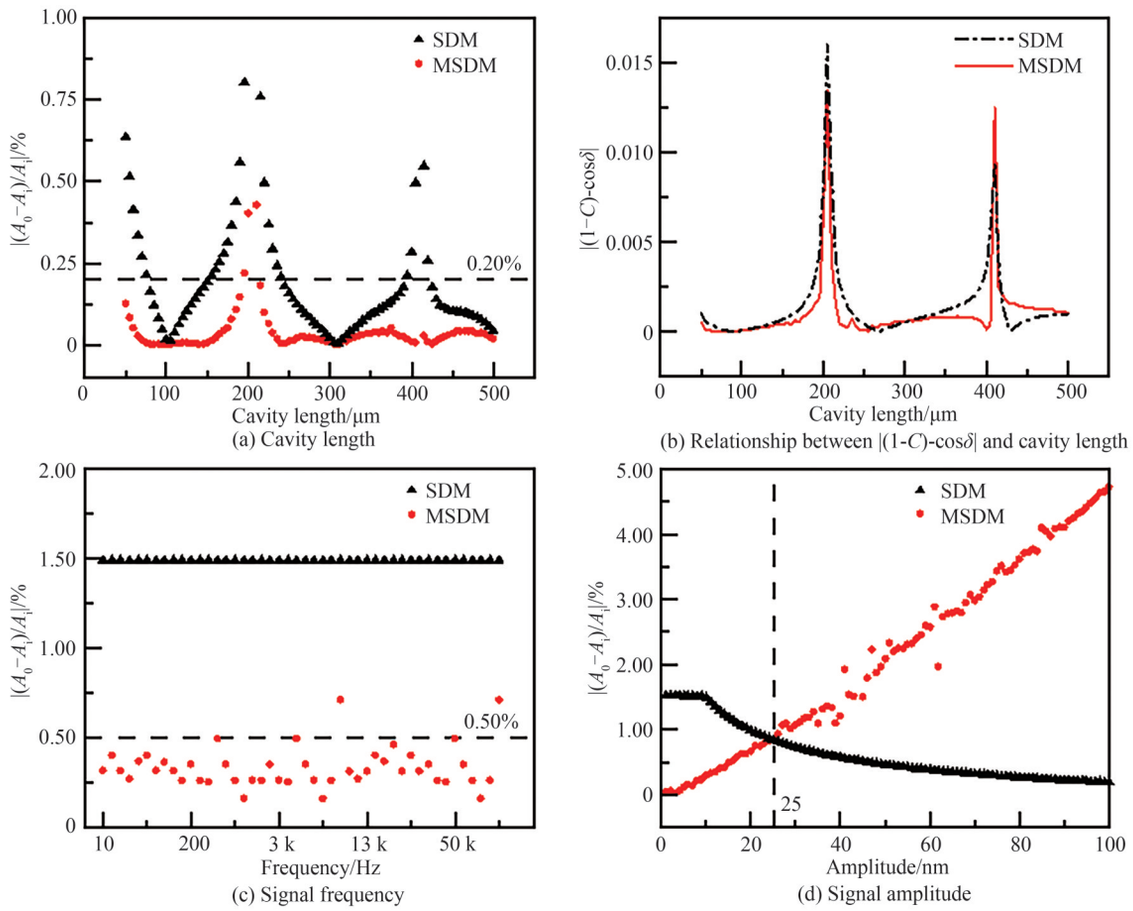

图4　两种方法解调误差随腔长、信号频率、信号幅度变化对比与cosδ误差

Fig.4　The demodulation error of the two methods varies with cavity length, signal frequency, amplitude and error of cosδ

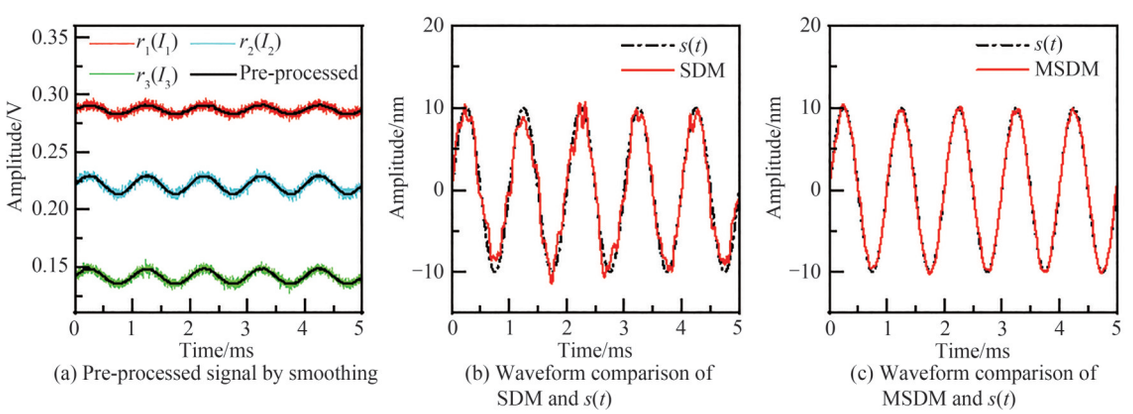

图5　仿真信号分别经过SDM与MSDM解调后的不同

Fig. 5　The result difference after demodulation by SDM and MSDM for simulation signal

4　实验测量

实验中选取的波长与仿真中相同，窄带滤波器的中心波长分别为$\lambda_1=1\,540.56$ nm、$\lambda_2=1\,541.35$ nm、$\lambda_3=1\,542.14$ nm，半峰全宽（Full Width at Half Maxima，FWHM）小于0.8 nm，系统所用的宽带光源是通过980 nm波长激光泵浦掺Er光纤制作的放大自发辐射光源（厦门彼格科技有限公司生产，型号：BG-ASE-SS-C）。光源的波长范围为1 526～1 563 nm，输出功率为10 dBm；PD单元为PIN光电二极管加放大电路，最大饱和功率为2 mW，对1 100～1 650 nm的光均有响应，最高响应频率为100 kHz，放大倍数可调；采集卡（汉泰6 074 BC）带宽70 MHz，垂直分辨率8 bit，输出数据的有效位数为小数点后4位，对于时基值为

500 μs、三路采集的情况，采样率为500 kHz。三路光信号的强度可通过调节放大电路的增益倍数使其尽可能与理论值相同。信号发生器（普源精电DG1022U）带宽25 MHz，采样率100 MHz，驱动扬声器发出声波。图6(a)为实验所用EFPI实物图，其腔长可通过其反射光谱曲线（图6(b)）的周期估算，约为205.18 μm。

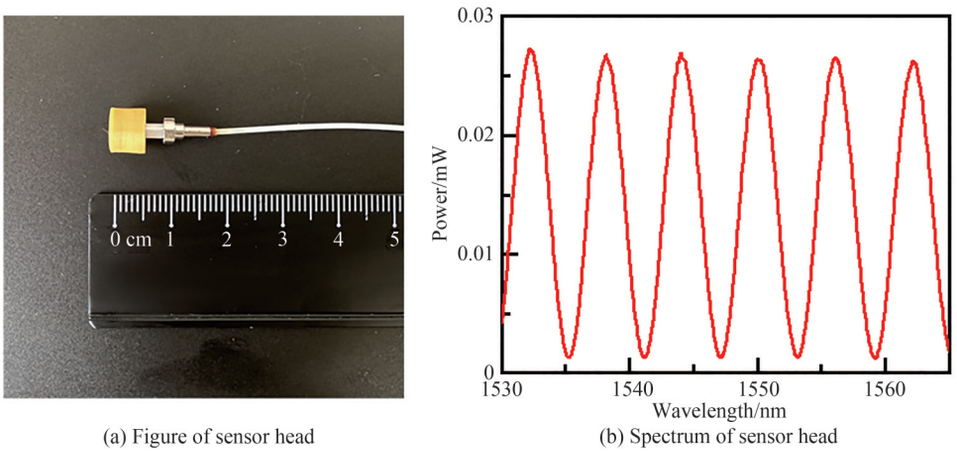

(a) Figure of sensor head　(b) Spectrum of sensor head

图6　EFPI探头的实物图与反射光谱

Fig. 6　Figure and spectrum of EFPI sensor head

信号发生器输出信号为1 kHz的正弦波，扬声器的等效声压为79.1 dB-SPL；采集卡接收到的信号见图7(a)，黑色曲线为高斯平滑之后的数据，三路信号质量最优时的信噪比均位于60～65 dB左右。可以看出，实验的结果与仿真具有良好的吻合：如图7(b)所示，SDM方法下，R_1的误差变大、波形变形，在波峰波谷位置出现较多的高频噪声。新方法MSDM的α与β通过对I_1、I_3分别进行和与差的运算，尽管β与R_2相同，但中间量α与β的大小关系始终相反：I_1与I_3反相时，α的幅值小于β的幅值；I_1与I_3同相时，α的幅值大于β的

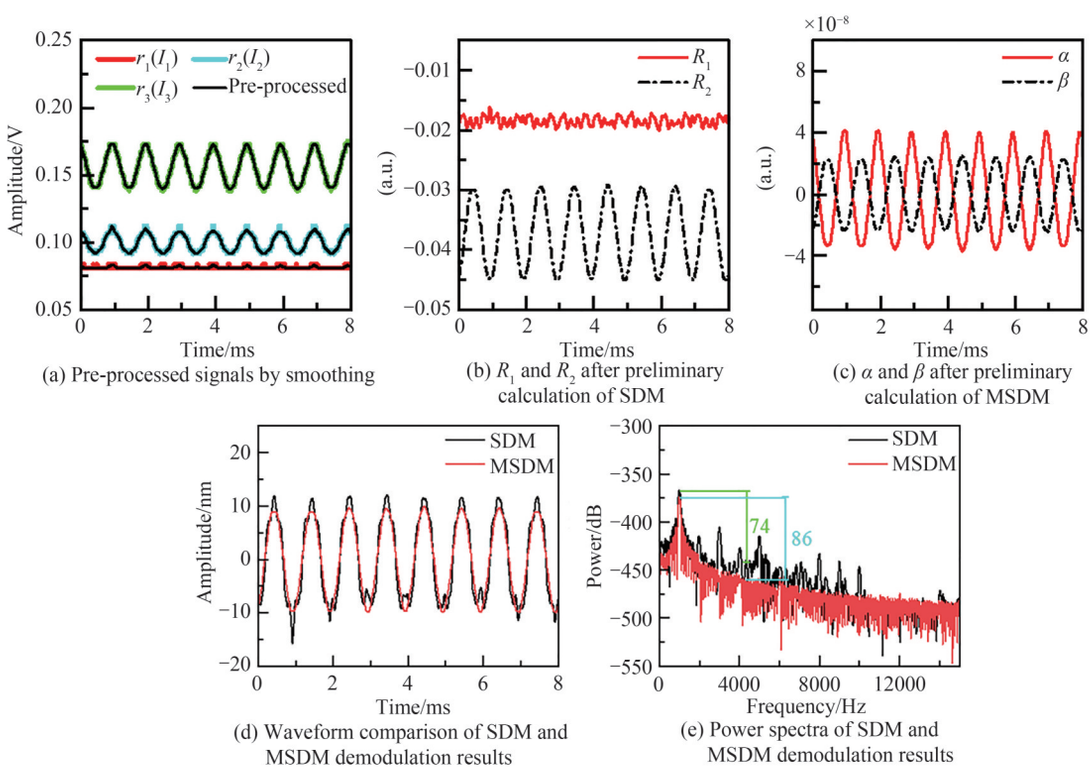

(a) Pre-processed signals by smoothing　(b) R_1 and R_2 after preliminary calculation of SDM　(c) α and β after preliminary calculation of MSDM

(d) Waveform comparison of SDM and MSDM demodulation results　(e) Power spectra of SDM and MSDM demodulation results

图7　相同信号分别经过SDM与MSDM解调后的不同

Fig.7　The difference after demodulation by SDM and MSDM for same signal

幅值，如图7(c)所示，这样就保证了α与β中的至少一个拥有更好的波形。图7(d)中可以看出，由于实际应用中噪声的构成复杂与SDM算法的高敏感性，SDM的解调结果在波峰波谷处出现了高频噪声，解调结果的信噪比变大；对于MSDM来说，β与R_2相同(图7(c))，但α的波形更好，图7(e)可见，MSDM有效提高了结果的信噪比，其功率谱相对SDM更加平滑，主频附近的信噪比从74 dB提高至86 dB。

图8是实验环境相同的条件下，其他三组任意时刻的R_1、R_2、α、β值，为了方便对比R_2与β的波形，R_2去除掉了直流部分，三个图中R_2与β几乎相同。图8(a)、(b)中，R_1的波形较差，图8(c)中当α波形较差时，β的波形则会相对更好。多次实验均可证明，α与β的构建可以保证其中至少一个中间量波形良好，再通过平方和算法扩大质量好的中间量在解调结果中的权重，以此实现更好的解调效果。

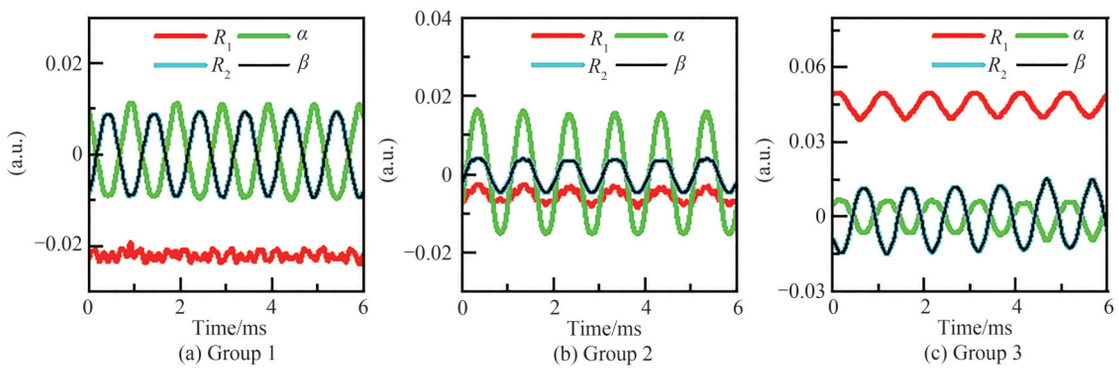

图8　多组实验中R_1、R_2、α、β的波形

Fig. 8　Waveforms of R_1, R_2, α, β in other experiment groups

腔长为200 μm左右的法珀腔，cosδ的值为0.67附近且随腔长的变化较为平缓(图9(a))，图9(b)是实验测得的cosδ值随声压的变化。随着声压的逐渐增加，由于扬声器功率不平稳与环境噪声、环境气压变化等随机误差的影响，cosδ的值尽管在波动，但始终维持在0.55～0.7之间，与理论值符合较好，侧面验证了算法的可靠性。同时，算法解调结果输出的幅值与声压之间也具有良好的线性，线性度达到0.995 11。图9(c)显示信号频率分别为100 Hz、500 Hz、1 kHz、10 kHz时，MSDM解调结果仍具有良好的信噪比。

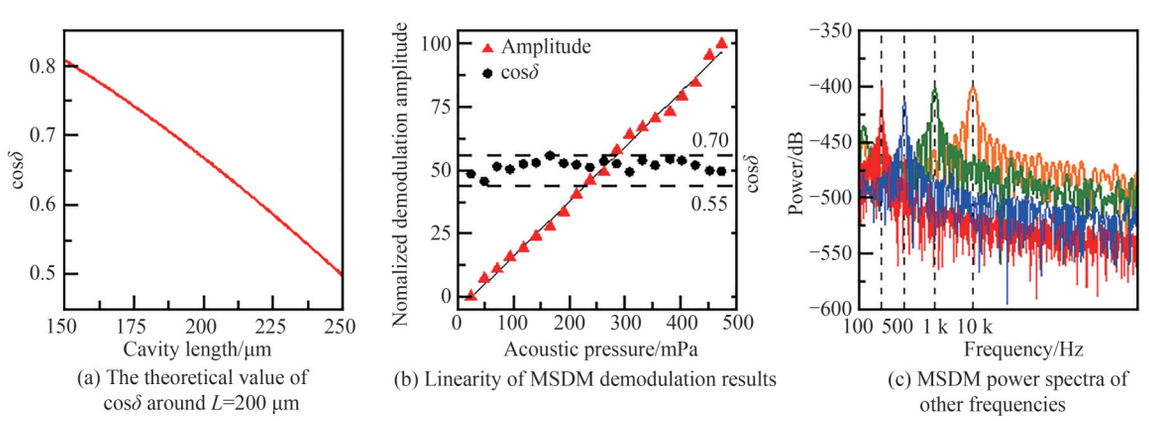

图9　腔长200 μm左右时cosδ理论值、声压与MSDM解调结果幅值线性度与其他频率下MSDM解调结果功率谱

Fig. 9　The theoretical value of cosδ when the cavity length is about 200 μm, the linearity between sound pressure and the amplitude of MSDM demodulation results and MSDM demodulation result spectra of other frequencies

5　结论

通过改进现有的对称三波长解调算法，提出了一种针对小信号的、恢复EFPI传感器接收信号的改进三波长解调方法。利用小信号情况下正弦函数的近似关系，通过三路信号的强度计算求得相位差，进而解决小信号条件下EFPI干涉信号的衰落问题。经过数值分析、仿真与实验，证明该方法在针对小信号的解调方

面具有更高的算法稳定性与更小的误差,对波形具有更好的恢复效果,且理论上也适用于非周期的小信号,有望在更多场景中得到应用。

参考文献

[1] WU Gaomi, XIONG Linsen, DONG Zhifei, et al. Development of highly sensitive fiber-optic acoustic sensor and its preliminary application for sound source localization[J]. Journal of Applied Physics, 2021, 129(16): 164504.

[2] XIA Zhenjie, LIU Qiang, LI Ang, et al. Sound source localization system based on diaphragm-type EFPI optical fiber microphones[J]. Chinese Journal of Lasers, 2021,48(9): 0910002.
夏振杰, 刘强, 李昂, 等. 基于膜片式EFPI光纤麦克风的声源定位系统[J]. 中国激光, 2021, 48(9): 0910002.

[3] XIONG Wanze, SHU Qian, LU Ping, et al. Sensitivity enhanced fiber optic hydrophone based on an extrinsic Fabry-Perot interferometer for low-frequency underwater acoustic sensing[J]. Optics Express, 2022, 30(6): 9307-9320.

[4] GAO Chaofei, YU Lei, XU Yue, et al. Partial discharge localization inside transformer windings via fiber-optic acoustic sensor array[J]. IEEE Transactions on Power Delivery, 2018, 34(4): 1251-1260.

[5] CAO Yingchun, JIN Wei, HO H L, et al. Miniature fiber-tip photoacoustic spectrometer for trace gas detection[J]. Optics Letters, 2013, 38(4): 434-436.

[6] KELLY L, CHEN Chen, BAO Xiaoyi, et al. High-resolution surface acoustic wave (SAW) strain sensor based on acoustic Fabry-Pérot resonance[J]. Sensors and Actuators A: Physical, 2022, 338: 113504.

[7] WANG Minyu, DONG Xiaopeng, ZHENG Yanmin, et al. Variation compensated of bias phase in M-Z interferometers with dual-wavelength method[J]. Journal of Optoelectronics·Laser, 2005(3): 294-297.
王民裕, 董小鹏, 郑艳敏, 等. 双波长补偿光纤M-Z干涉仪偏置相位漂移[J]. 光电子·激光, 2005(3): 294-297.

[8] ZHANG Wanjin, LU Ping, QU Zhiyuan, et al. Four-wavelength quadrature phase demodulation technique for extrinsic Fabry-Perot interferometric sensors[J]. Optics Letters, 2022, 47(10): 2406-2709.

[9] ZHANG Xiongxing, WANG Wei, CHEN Haibin, et al. Two-parameter elliptical fitting method for short-cavity fiber Fabry-Perot sensor interrogation[J]. Sensors, 2018, 19(1): 36.

[10] LIU Qiang, JING Zhenguo, LI Ang, et al. Common-path dual-wavelength quadrature phase demodulation of EFPI sensors using a broadly tunable MG-Y laser[J]. Optics Express, 2019, 27(20): 27873-27881.

[11] QIAN Heng, LUO Bin, HE Haijun, et al. Phase demodulation based on DCM algorithm in Φ-OTDR with self-interference balance detection[J]. IEEE Photonics Technology Letters, 2020, 32(8): 473-476.

[12] DONG Zhifei, HU Xinyu, REN Dipeng, et al. Judgment and compensation of deviation of the optical interferometric sensor's operating point from the interferometer quadrature point[J]. Journal of Lightwave Technology, 2021, 39(21): 7008-7017.

[13] ZHANG Yabin, SUN Xintong, CAO Jianian, et al. Demodulation features of different types of signals for fiber-optic sensors[C]. Advanced Sensor Systems and Applications IV, SPIE, 2010, 7853: 66-70.

[14] ZHAO Jianghai, SHI Yikai, SHAN Ning, et al. Stabilized fiber-optic extrinsic Fabry-Perot sensor system for acoustic emission measurement[J]. Optics & Laser Technology, 2008, 40(6): 874-880.

[15] ZHANG Shuhuan, JIANG Yi. Phase demodulation method for non-periodic signal in extrinsic Fabry-Perot interferometric sensor[J]. Acta Optica Sinica, 2022, 42(9): 81-86.
张树桓, 江毅. 非本征法布里-珀罗干涉型传感器非周期信号的相位解调方法[J]. 光学学报, 2022, 42(9): 81-86.

[16] LIU Bin, LIN Jie, LIU Huan, et al. Diaphragm based long cavity Fabry-Perot fiber acoustic sensor using phase generated carrier[J]. Optics Communications, 2017, 382: 514-518.

[17] JIA Jingshan, JIANG Yi, HUANG Junbin, et al. Symmetrical demodulation method for the phase recovery of extrinsic Fabry-Perot interferometric sensors[J]. Optics Express, 2020, 28(7): 9149-9157.

[18] YU Wenjian. Numerical analysis and algorithms[M]. Beijing: Tsinghua University Express, 2020: 6-25.
俞文健. 数值分析与算法[M]. 北京: 清华大学出版社, 2020:6-25.

[19] SHENG Qiwen, LIU Guigen, UDDIN N, et al. Analysis of single-mode fiber-optic extrinsic Fabry-Perot interferometric sensors with planar metal mirrors[J]. Applied Optics, 2021, 60(26): 7894-7902.

[20] LIN Shengtao, WANG Zinan, XIONG Ji, et al. Rayleigh fading suppression in one-dimensional optical scatters[J]. IEEE Access, 2019, 7: 17125-17132.

A Modified Three-wavelength Demodulation Method for Small Signals of EFPI

YANG Ruimu, DONG Xiaopeng

(*Institute of the Lightwave Technology, School of Electronic Science and Engineering, Xiamen University, Xiamen* 361000, *China*)

Abstract: Fiber optic Extrinsic Fabry-Perot Interferometers (EFPI) are frequently utilized in many acoustic sensing scenarios due to their simple structure, ease of fabrication, high sensitivity, high phase consistency, and strong resistance to electromagnetic interference. However, the cavity length of the EFPI sensor is susceptible to environmental variables such as temperature and air pressure, and the drifting of the orthogonal working point caused by the change of cavity length will lead to signal fading and distortion. Nevertheless, several demodulation methods are less practical or even ineffective when dealing with small signals: Dual-wavelength method for Mach-Zehnder interferometer is inconvenient to apply to the EFPI demodulation; the Ellipse-Fitting Algorithm′s (EFA) Lissajous figure will degenerate into a straight line for small signals, and there are also the disadvantages of poor real-time performance and slow demodulation speed; the second-order Differentiate-and-Cross-Multiply (DCM) operation has wide applicability, but the Direct Current (DC) term must be accurately removed, for small signals, the removal of DC term is difficult; the Bessel method has the same difficulties as DCM, and it can only demodulate single-frequency signals; The method of using tunable laser feedback to control the orthogonal working point has the drawback of high cost, and lasers with wavelength scanning function have high requirements for hardware reliability; Phase Generated Carrier (PGC) technology requires a complex carrier modulation system with a limited frequency response range, and the system is complex and large when PGC uses piezoelectric transducer to generate phase carriers. In contrast, intensity demodulation has the advantages of a linear transfer function, simple signal processing, high sensitivity and is suitable for the detection of high-speed and small signal. JIANG Yi et al. proposed a Symmetrical Demodulation Method (SDM) suitable for unstable cavity length and unknown cavity length, which constructs two equal interference phase differences between the three output signals by selecting specific three wavelengths, and then recovers the phase of the signal through mathematical operations. This method has the advantages of large dynamic range and simple operation, and it is more suitable for the detection of large signals. However, in the case of small signals, the SDM algorithm may lead to increased noise and error in the demodulation result.

If the wavelength of the light source is 1 550 nm, the interference phase of EFPI changes $0\sim2\pi$, corresponding to the cavity length variation range of 775 nm. When the cavity length change caused by vibration is less than 30.11 nm, that is, the radian value in the interference phase is less than 0.22 rad, the approximate error of $\sin x$ and x is less than 1%. Under this condition, we can directly remove the DC term of interference signal reflected by EFPI to avoid the difficulty of distinguishing DC terms in small signals, $B\sin\varphi\dfrac{4\pi ns(t)}{\lambda}$ can be regarded as the approximation of an interference signal. Three specific wavelengths are selected to construct two equal interference phase differences between the three output signals, and on the basis of these three signals, the two intermediate formulas can be compensated for each other to avoid the cancellation phenomenon, it ensure that at least one of the intermediate formulas has a better waveform, so as to obtain an intensity demodulation result with better Signal-To-Noise Ratio (SNR) and this approach is summarized as a Modified Symmetrical Demodulation Method (MSDM).

Both theoretical analysis and numerical simulation demonstrate that MSDM performs better than SDM for small signals. Theoretical analysis indicates MSDM has a smaller and smoother error bound and relative condition number than SDM. In the numerical simulation, MSDM has less error than SDM in cavity length, frequency, and signal amplitude. After adding Gaussian white noise to the simulated signal, more high-frequency noise appears in SDM, while MSDM achieves superior demodulation results for the signal waveform. In the experiment, the SNR of the three signals ranges from 60~65 dB, and the experiment results align well with the simulation. Due to the complicated noise in practical applications and the high sensitivity of SDM, high-frequency noise appears in the demodulation results of SDM, resulting

in a decrease in SNR. MSDM effectively improves the SNR of the demodulation results, the power spectra of MSDM′s results are smoother than those of SDM, and the SNR near the main frequency increases from 74 dB to 86 dB. Values of cosδ measured in experiments consistently maintain between 0.55～0.7, in agreement with the theoretical predictions, thus confirming the reliability of MSDM. Additionally, the outputs of MSDM perform good linearity with the sound pressure of the speaker, and the linearity coefficient reaches 0.995 11. When the signal frequencies are 100 Hz, 500 Hz, 1 kHz, and 10 kHz, respectively, the MSDM demodulation results still have good SNR.

An improved three-wavelength demodulation method for small signals of EFPI sensors is proposed by enhancing the existing three-wavelength phase demodulation algorithm. Our research group uses the approximate relationship of the sinusoidal function under small signal conditions to calculate the phase difference by calculating the intensity of the three signals, thereby solving the fading problem of EFPI interference signals. Through numerical analysis, simulations and experiments, it is proved that the proposed method has higher algorithm stability and smaller error in demodulation for small signals and better recovery on waveforms. Besides, the algorithm also theoretically has certain demodulation capabilities for non-periodic signals, which can potentially expand its application in the future.

Key words: Extrinsic Fabry-Perot interferometers; Three-wavelength demodulation; Signal Fading; Acoustic detection; Small signal

OCIS Codes: 060.2370; 120.2230; 280.4788

Foundation item: National Natural Science Foundation of China (No. 61775186), the Marine and Fisheries Bureau of Xiamen under Project (No. 16CZB025SF03), Key Laboratory for Optical Communication Device Test of Xiamen